Journal Pre-proof

Fabrication of skinless cellular poly (vinylidene fluoride) films by surface-constrained supercritical CO$_2$ foaming using elastic gas barrier layers

Lin Wang, Wenhao Cui, Hao-Yang Mi, Dongdong Hu, Maxwell Fordjour Antwi-Afari, Chuntai Liu, Changyu Shen

Please cite this article as: Lin Wang, Wenhao Cui, Hao-Yang Mi, Dongdong Hu, Maxwell Fordjour Antwi-Afari, Chuntai Liu and Changyu Shen, Fabrication of skinless cellular poly (vinylidene fluoride) films by surface-constrained supercritical CO$_2$ foaming using elastic gas barrier layers, *The Journal of Supercritical Fluids,* (2021) doi:https://doi.org/10.1016/j.supflu.2022.105562

This is a PDF file of an article that has undergone enhancements after acceptance, such as the addition of a cover page and metadata, and formatting for readability, but it is not yet the definitive version of record. This version will undergo additional copyediting, typesetting and review before it is published in its final form, but we are providing this version to give early visibility of the article. Please note that, during the production process, errors may be discovered which could affect the content, and all legal disclaimers that apply to the journal pertain.

Fabrication of skinless cellular poly (vinylidene fluoride) films by surface-constrained supercritical CO₂ foaming using elastic gas barrier layers

Lin Wang[a], Wenhao Cui[a], Hao-Yang Mi[a]*, Dongdong Hu[b],

Maxwell Fordjour Antwi-Afari[c], Chuntai Liu[a], Changyu Shen[a]

[a] Key Laboratory of Materials Processing & Mold, Ministry of Education; National Engineering Research Center for Advanced Polymer Processing Technology, Zhengzhou University, Zhengzhou, 450000, China

[b] Shanghai Key Laboratory of Multiphase Materials Chemical Engineering, East China University of Science and Technology, Shanghai 200237, China

[c] Department of Civil Engineering, College of Engineering and Physical Sciences, Aston University, Birmingham, B4 7ET, United Kingdom

Corresponding authors:

H.Y. Mi: mihaoyang@zzu.edu.cn

Abstract

Removing the solid skin of polymer foams is a challenging approach for supercritical carbon dioxide (scCO₂) foaming. Herein, a surface-constrained foaming method was used to fabricate skinless cellular poly (vinylidene fluoride) (PVDF) films. The use of organosilicone and nature latex as gas barrier layers resulted in low CO₂

1

diffusion rates of 2.16×10^{-11} m^2/s and 4.73×10^{-13} m^2/s, and trigger heterogeneous nucleation of cells on the PVDF/barrier layer interface. The skin layer and the cell size gradient in the region close to the surface were successfully eliminated, and the surface cell density and cell size could be controlled in the range of 7.2×10^6 cells/cm^3, and 13~41 μm, respectively. Moreover, the fabricated skinless cellular PVDF films exhibited an enhanced melting temperature and crystallinity due to the plasticizing effect of scCO$_2$. The present study provides new thoughts for the fabrication of skinless polymer films using surface-constrained scCO$_2$ foaming.

Keywords: Poly (vinylidene fluoride); Supercritical CO$_2$ foaming; Skin layer; Porous structure; Thermal property.

1. Introduction

Fabrication of polymer foams using supercritical fluids such as supercritical carbon dioxide (scCO$_2$) and nitrogen (N$_2$) as blowing agents is an efficient and environmentally friendly technique that has been increasingly used in the production of foams for various applications, including electromagnetic interference shielding [1, 2], oil absorbents [3-5], triboelectric nanogenerator [6, 7], and thermal insulation [8, 9]. Polymer films with highly porous structures have shown tremendous potential in advanced novel techniques such as gas sensors [10, 11], on-skin electrons devices [12, 13], flow batteries [14, 15], radiative cooling [16], and biomedicine [17-19]. Cellular polymer films are normally prepared via phase separation [20], controlled etching [21], particulate leaching [22], and fiber bonding [23]. Most of these methods require a large amount of organic solvent and water, which are energy inefficient and may cause potential water pollution [24, 25].

2

ScCO$_2$ foaming could be a feasible solution to realize low-cost green fabrication of cellular polymer films. In gas foaming process, the polymer matrix is saturated with scCO$_2$ under high pressure and temperature. The cells are formed in the depressurization stage due to thermodynamic instability caused by the transformation of carbon dioxide (CO$_2$) from a supercritical state to a gas state [26]. However, CO$_2$ dissolved in the region close to the surface of the polymer would escape from the polymer matrix when the pressure is suddenly reduced, thus, led to the formation of a solid skin layer on the polymer foams [27, 28]. Furthermore, the rapid escape of CO$_2$ can make it difficult to produce cellular polymer films with high porosity [29]. Therefore, eliminating the skin layer can be a challenging approach for scCO$_2$ foaming to extend their applicable fields.

Blade trimming is a typical approach used in the industrial production of polymer foams to remove solid skin layers. It not only requires an additional process but also increases the waste material and the total cost. Using a co-blowing agent of CO$_2$ and water has shown the ability to greatly reduce the thickness of the skin layer for thermoplastic polyurethane (TPU) foams by plasticizing the molecular chains [30]. However, the number of cells formed on the surface of the foamed sample has been low. Another approach to create cells on the foam surface is by introducing a water-soluble immiscible phase in the polymer matrix followed by CO$_2$ foaming and leaching of the sacrificial phase [31]. Although the etched water-soluble phase would leave out channels on the foam surface, the major areas on the surface could still be solid.

Surface-constrained foaming is an approach that uses gas barrier films to limit the diffusion rate of CO$_2$ from polymer matrix. Siripurapu et al. [32] developed a surface-mediated foaming process by using stainless-steel plates to regulate CO$_2$ diffusion only in

the edge of polymethyl methacrylate (PMMA) films, which resulted in the formation of porous structure in PMMA thin film. However, the morphology of the film surface was not reported. Ge et al. [33, 34] prepared foamed TPU membranes with perforation or holes by introducing two polyimide (PI) films on both sides of a thin TPU film and realized that the formation of uniform cells on the surface of TPU film was due to an enhanced cell nucleation at the PI/TPU interface. Li et al. [35] investigated the influence of surface-constrained layers on the foaming behavior of TPU film using PI and poly (ethylene terephthalate) (PET) as the gas barrier layers. The hydrogen bonding between TPU and PI resulted in tight adhesion and effectively removed the skin layer, while the PET film was disassociated during the foaming process because of low adhesion. Although PI film seems to be a good gas barrier material with high adhesion to TPU, it is limited to the expansion of TPU foam in the direction parallel to PI film due to its high stiffness. In addition, it may be unsuitable for surface-constrained foaming of other polymers that have low surface energy such as polyvinylidene fluoride (PVDF).

Cellular PVDF films are widely used in the applications of oil/water separation [36], filtration [37], heat insulating [38], and dielectric membranes [39]. They are typically produced by phase inversion using organic solvents. Green fabrication of cellular PVDF films using surface-constrained $scCO_2$ foaming is highly desired for practical production. Zhao et al. [38] prepared foamed PVDF with tailored microcellular structures by batch-foaming to obtain ultra-low dielectric constant and thermal conductivity. Lee et al. [40] abricated microcellular PVDF/multiwalled carbon nanotube (MWCNT) nanocomposite foam by $scCO_2$ bead foaming. Wong et al. [41] demonstrated PVDF with high porosity (49~95 %) and closed or interconnected pores using liquid foams stabilized by polymeric

particles. Yang et al. [42] prepared a three-dimensional porous PVDF with improved piezoelectric output by a facile strategy coupling selective laser sintering (SLS) and scCO$_2$ foaming. However, there are rare previous studies that reported the formation of cells on surface of PVDF and techniques to eliminate the skin layer of PVDF foams.

In this study, to realize the foaming of PVDF film and the elimination of solid skin layer, two barrier materials including organosilicone and nature latex were used as the gas barrier materials in addition to PI. Both organosilicone and nature latex are elastic materials that can be in situ synthesized on the surface of PVDF film, which may have tight adhesion to PVDF and can be expanded during the PVDF foaming. The effects of surface-constrained material on the foaming behavior of PVDF film were investigated in detail. The morphologies on the surface and in the cross-section of different foams were also compared. The elastic gas barrier layers outperformed the PI film in removing the skin layer and created a porous structure on the film surface. The underlying mechanism was analyzed and elaborated to provide general guidance. In addition, the skinless cellular PVDF films exhibited superior thermal properties than the conventional PVDF foam.

2. Experimental Procedure

Materials

PVDF (Kynar 720) with a purity of 99.9% was supplied from Aohua Plastics Co., Ltd. (Shanghai, China). The physical property of PVDF is shown in Table S1. Polyimide (PI) films with a thickness of 100 μm were supplied by Shanghai Feilbo Co., Ltd, China. Organosilicone with a Shore hardness of 50 A was purchased from Fanhe Trading Co.,

Ltd. (Shanghai, China). Nature latex was purchased from Dongguan Yonghe Rubber Co., Ltd, China. The CO_2 with a purity of 99.9% was obtained from Zhengzhou Yumeng Gas, Co., China, and used as the physical blowing agent.

Preparation of surface-constrained PVDF films

PVDF pellets were dried at 60 °C in a vacuum oven for 6 h to remove moisture. Sandwich structured PI/PVDF/PI films with a thinness of 500 μm were prepared by vacuum-assisted hot compression. Briefly, PVDF pellets were evenly dispersed onto a PI film (1.5 cm × 3 cm) and covered with another PI film followed by compression molding at 220 °C under 10 MPa for 10 min and cooling at 70 °C under pressure.

Organosilicone enclosed PVDF (OS/PVDF/OS) films were prepared by coating PVDF films with organosilicone solution which comprised of the silicone base (part A) and crosslinker (part B) followed by curing at room temperature for 3 h. The thickness of the organosilicone layer was about 100 μm.

Similarly, nature latex enclosed PVDF (NL/PVDF/NL) films were prepared by coating PVDF films with latex solution which comprised of nature latex solution and curing agent for few seconds. The thickness of the latex layer was controlled to about 100 μm by repetitive coating.

Preparation of skinless cellular PVDF films

To prepare cellular PVDF films, PI/PVDF/PI, OS/PVDF/OS, and NL/PVDF/NL films with a size of 1.5 cm × 3 cm were sealed in a stainless steel chamber and flushed with low-pressure CO_2 for 2 min to eliminate the air in the chamber. Then, the

temperature was raised to different levels (163 °C and 166 °C) followed by charging with high-pressure $scCO_2$ to different pressures (16 MPa and 20 MPa). Samples were saturated with $scCO_2$ for 2 h to reach solubility equilibrium followed by rapidly reducing the pressure to atmospheric pressure in 3 s to allow the foaming of PVDF. Samples were taken out from the chamber rapidly and naturally cooled to room temperature. The constrained layers (PI film, organosilicone film, and nature latex film) were slowly peeled off from the foamed samples to obtain skinless cellular PVDF thin films. The foaming temperatures of 163 °C and 166 °C were studied because of the small foaming window of PVDF. When the temperature is too low (e.g., 160 °C) or too high (e.g., 169 °C), the PVDF would be either solid or dominated by collapsed cells as shown in Figure S1.

Characterizations

Scanning electron microscopy (SEM, JEOL, Japan) was used to observe the surface morphology and porous structure of different samples at an operating voltage of 20 kV. The films were frozen in liquid nitrogen for 20 min and fractured using clamps, followed by coating with a thin film of gold before observation. The cell size and cell density were measured from the SEM images using Image-Pro Plus software. The average cells size was obtained by averaging the diameters of at least 100 cells of the SEM images and the cells density was calculated by using Equation (1),

$$N_f = \left[\frac{nM^2}{A} \right]^{3/2} \tag{1}$$

Where, n is the number of cells in a micrograph with the area of A (cm^2) and M is the magnification factor.

7

Differential scanning calorimeter (DSC) measurements were performed via a DSC Q2000 instrument to evaluate the thermal behavior of raw PVDF and cellular PVDF films. Approximately 5 mg samples were encapsulated in a standard aluminum pan and heated to 250 °C at the heating rate of 10 °C/min in a nitrogen atmosphere. After keeping the temperature at 250 °C for two minutes to remove the thermal history, the samples were cooled to ambient temperature at the same rate. The sample of raw PVDF films was heated to 250 °C, again at the same scanning rate of 10 °C/min. The melting temperatures (T_m) were measured from the endothermic peak in the heating curves. The corresponding degree of the crystallinity (χ_c) was calculated according to Equation (2),

$$\chi_c = \frac{\Delta H_f}{\Delta H_f^*} * 100\%$$
(2)

Where, ΔH_f is the melting enthalpy of the measured PVDF sample, ΔH_f^* represents the melting enthalpy of PVDF with 100% crystallinity, which is about 104.5 J/g [43].

3D Super Depth Digital Microscope (Leica DVM6) was used to observe the cross-sectional morphology. Sandwiched samples were fractured in cross-section and the interfacial bonding between PVDF and constrained layers were analyzed.

Labthink BTY-B2P was used to measure the CO_2 permeability of constrained layers (PI film, organosilicone film, and nature latex film) by measuring the mass of CO_2 passed within 24 h at a pressure of 0.1 MPa under ambient conditions. The samples of constrained layers were circular films with a thickness of 1 mm and a diameter of 30 mm. The permeability coefficient was calculated according to the time–pressure curve. The diffusivity (D) was calculated by using Equation (3).

$$D = \frac{I^2}{6\theta}$$
(3)

8

Where, *I* represents the membrane thickness, θ is the time lag, intercept of the asymptotic line of the time–pressure curve to the time axis.

The adhesion strength between PI, organosilicone, nature latex, and PVDF layers was evaluated in terms of T-peel force. The test was carried out by tensile mode using a test machine (UTM2203, Shenzhen Suns Technology Stock Co., Ltd., China). To obtain accurate data, the sample was cut into strips with a size of 15 mm $\times$ 30 mm and an effective bonding length longer than 5 mm. The average value of the stable data during the plateau-like period is used to represent the peel strength. The peeling speed was 4 mm/min, and the data used was the average of three results.

3. Results and discussion

3.1 Surface morphology of skinless cellular PVDF films

Aiming to eliminate the skin layer of cellular PVDF films, it is desired to restrict the escaping CO_2 and the rupture of cells on the film surface. Here, PI film, organosilicone, and nature latex were chosen as gas barriers in the $scCO_2$ foaming process to constrain the CO_2 dissipation. As illustrated in Figure 1, sandwich structured PI/PVDF/PI, OS/PVDF/OS, NL/PVDF/NL preform films were prepared by hot compression or surface coating methods followed by $scCO_2$ foaming at different temperatures and pressure. Constrained materials were removed from the foamed samples to obtain the skinless cellular PVDF films. The effects of the surface-constrained materials and the processing conditions on the morphology of cellular PVDF films as well as the underlying mechanism were investigated in detail.
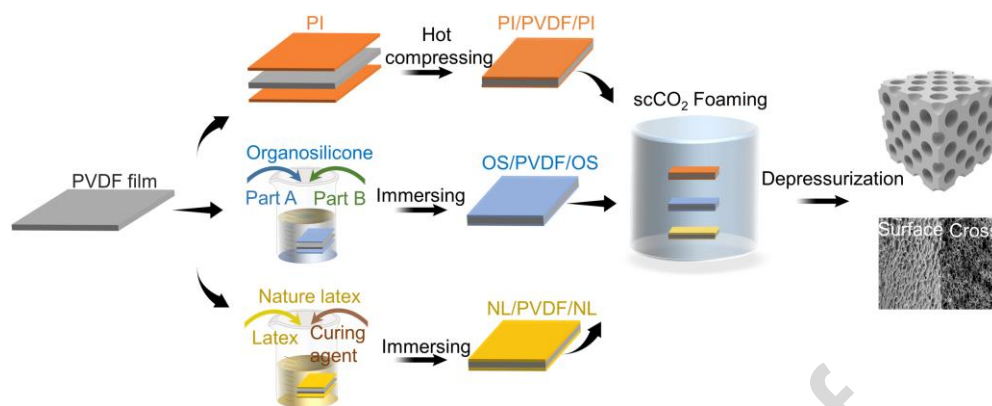
Figure 1. Schematic illustration of the fabrication process of skinless cellular PVDF films using PI, organosilicone, and nature latex as surface-constrained materials.

The surface morphology and the morphology in the side view of different cellular PVDF films were investigated using SEM. When foamed at 163 °C under 16 MPa, it was found from Figure 2 that neat PVDF (Figure 2a) and PI/PVDF/PI (Figure 2b) films displayed solid skin layers and few voids were observed on the surface of PI/PVDF/PI film. Spare shallow cells were observed on the surface of OS/PVDF/OS film (Figure 2c), while substantial cells were presented on the surface of NL/PVDF/NL film as shown in Figure 2d. From the side view, it is evident that the neat PVDF was barely foamed (Figure 2e), the PI/PVDF/PI film (Figure 2f) had a skin layer thickness of 25 μm with smaller cells close to the skin layer, the OS/PVDF/OS film (Figure 2g) showed a skin layer thickness of 15 μm with a large solid area on the surface, and the skin layer of the NL/PVDF/NL film (Figure 2h) was hard to distinguish. In addition, the cells on the surface were not interconnected with the cells inside.
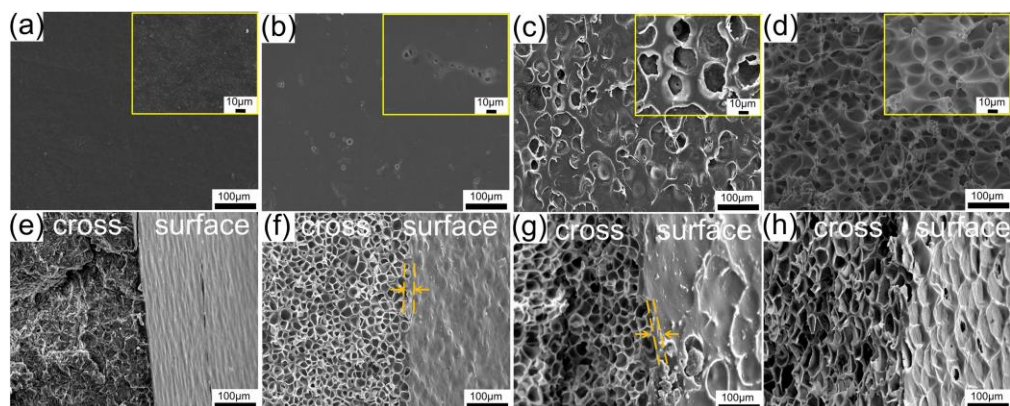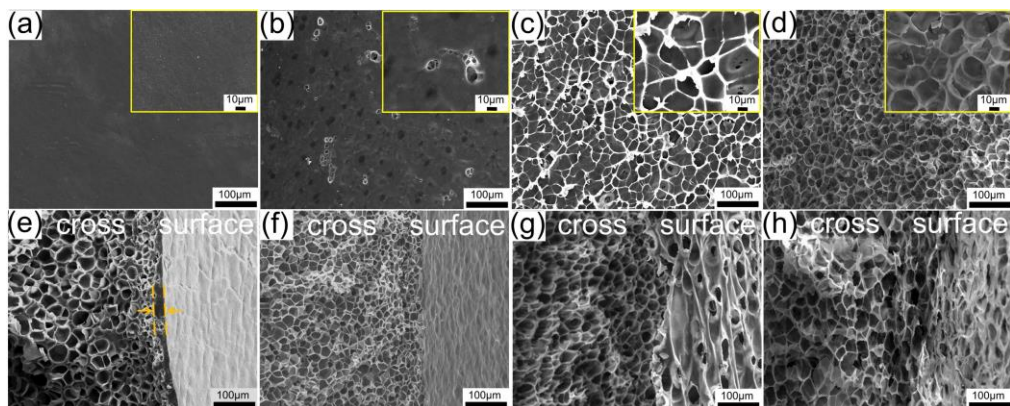
Figure 2. SEM micrographs (a-d) on the surface and (e-h) from the side view of (a, e) Neat PVDF, cellular (b, f) PI/PVDF/PI, (c, g) OS/PVDF/OS, (d, h) NL/PVDF/NL films fabricated at foaming condition of 163 °C and 16 MPa.

Figure 3 shows the SEM images of cellular PVDF films prepared at an increased pressure of 20 MPa while maintaining the same temperature at 163 °C. When foamed under elevated pressure, neat PVDF (Figure 3a) and PI/PVDF/PI (Figure 3b) still displayed solid skin layers with skin layer thicknesses of 44 μm and 10 μm, respectively. Remarkably, OS/PVDF/OS film exhibited a highly porous surface morphology with the skin layer completely removed (Figures 3c and 3g). In the case of NL/PVDF/NL film, the cells formed on the surface were highly connected, and cell merging was also observed (Figure 3d). In addition, the cells on the surface were mostly connected with the cells inside (Figure 3h). These results suggested that high foaming pressure is favorable for triggering the nucleation and formation of cells on the constrained surface, and the gas barrier materials had a great influence on the cellular structure on the surface.

11
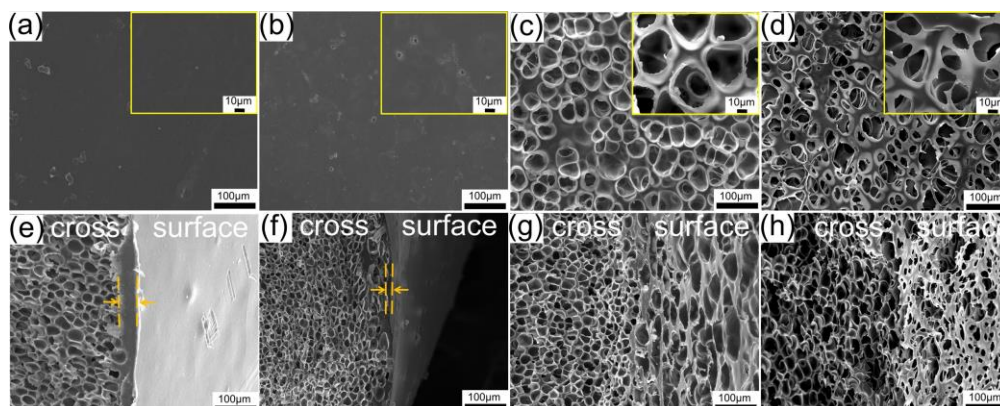
Figure 3. SEM micrographs (a-d) on the surface and (e-h) from the side view of (a, e) Neat PVDF, cellular (b, f) PI/PVDF/PI, (c, g) OS/PVDF/OS, (d, h) NL/PVDF/NL films fabricated at foaming conditions of 163 °C and 20 MPa.

To enhance the expansion ratio, different PVDF films were foamed at 166 °C under 20 MPa. As shown in Figure 4, all foams achieved larger cell sizes when foamed at elevated temperatures. Nevertheless, the neat PVDF remained a solid skin layer with a thickness of 24 μm (Figures 4a and 4e). Although few cells appeared on the surface of PI/PVDF/PI film as shown in Figure 4b, the skin layer is still obvious when observed from the side view (Figure 4f). The cells on the surface of OS/PVDF/OS film displayed polygon shapes with thin cell walls, and many of them were interconnected with each other as shown in Figure 4c. The NL/PVDF/NL film showed a porous surface morphology with a high cell density (Figure 4d). The skin layer was absent on both OS/PVDF/OS and NL/PVDF/NL films. Therefore, the organosilicone rubber and nature latex are preferred gas barrier materials for the foaming of PVDF films to eliminate the solid skin layer.

Figure 4. SEM micrographs (a-d) on the surface and (e-h) from the side view of (a, e) Neat PVDF, cellular (b, f) PI/PVDF/PI, (c, g) OS/PVDF/OS, (d, h) NL/PVDF/NL films fabricated at foaming conditions of 166 °C and 20 MPa.

The average cell size and cell density results on the surfaces of cellular OS/PVDF/OS and NL/PVDF/NL films were measured and compared (Figure 5) to analyze the effect of surface constrained material and foaming conditions. It was found that both cell size and cell density had the same trend for OS/PVDF/OS and NL/PVDF/NL films with changes in foaming conditions. When the foaming pressure was increased from 16 to 20 MPa with the temperature kept at 163 °C, the cell size was increased along with the decrease of cell density. However, when the foaming temperature was enhanced from 163 °C to 166 °C, the average cell size was reduced, and the cell density was greatly increased. By comparing cellular OS/PVDF/OS and NL/PVDF/NL films, it was obvious that cellular OS/PVDF/OS film had greater cell size and smaller cell density than cellular NL/PVDF/NL film.
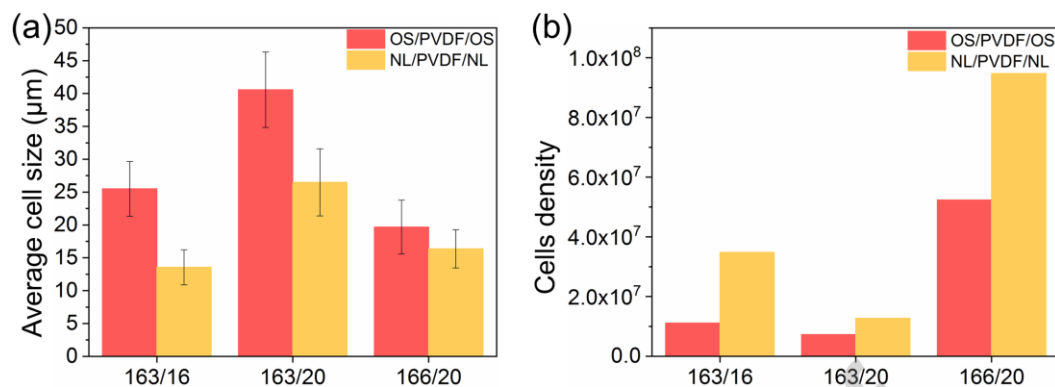
Figure 5. (a) Average cell size and (b) cell density on the surface of skinless cellular PVDF films prepared by using organosilicone or nature latex as constrained layers under different foaming conditions.

3.2. Cross-sectional morphology of skinless cellular PVDF films

Figure 6 shows the cross-sectional morphology of different cellular PVDF films foamed under different conditions. When foamed at 163 °C under 16 MPa, it was found that neat PVDF (Figure 6a) film displayed a solid core without visible cells. Conversely, all surface-constrained films displayed cellular morphology when foamed under the same condition. The average cell size and cell density results are shown in Figure 7. It was found that NL/PVDF/NL film had the largest cell size and lowest cell density, while PI/PVDF/PI film had a much higher cell density and smaller cells than the other cellular films. When the foaming pressure was increased to 20 MPa (Figure 6a$_2$-d$_2$), neat PVDF film was foamed and displayed a uniform cellular structure with a larger cell size and smaller cell density than other surface-constrained cellular PVDF films. Among the surface-constrained cellular PVDF films, NL/PVDF/NL still had the largest cell size and lowest cell density, and PI/PVDF/PI film had the smallest cell size and highest cell density. When the foaming temperature was increased to 166 °C (Figure 6a$_3$-d$_3$), the

14

trend of cell size and cell density were the same. Therefore, high foaming pressure is favorable for enhancing the cell density, and increasing foaming temperature is beneficial for improving the cell size [44]. The basic conclusions are the same in the surface-constrained foaming process. When comparing different surface-constrained cellular PVDF films, it was found that the nature latex constrained layer is favorable for the formation of large cells in the cross-section, while cellular films with PI constrained layers tend to form smaller cells with high cell density. The cell size and density of cellular films with organosilicone constrained layers were located between them.
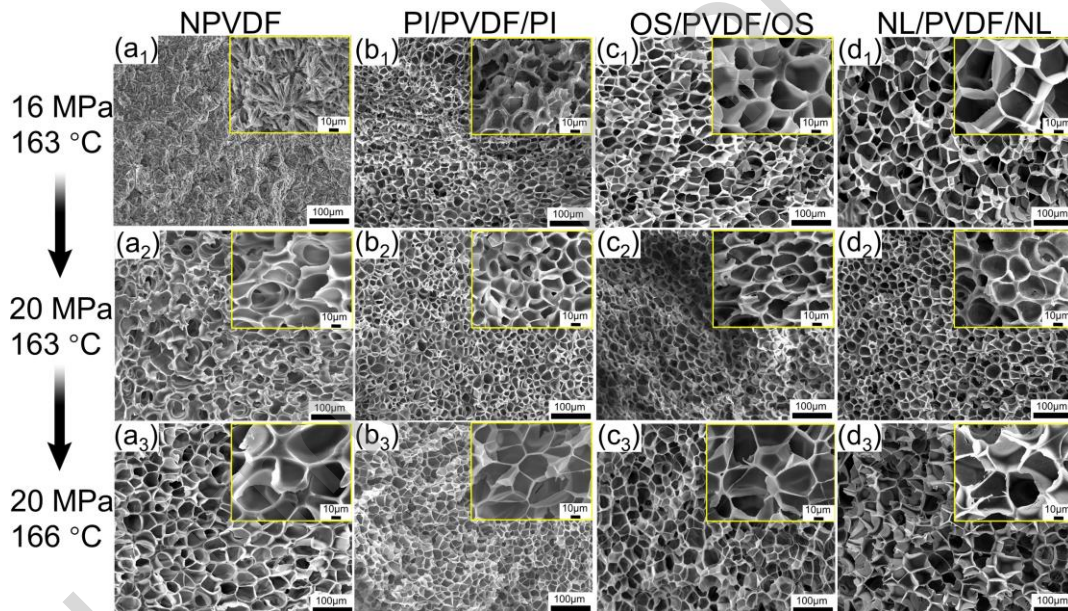
Figure 6. Cross-sectional SEM micrographs of (a) neat PVDF, cellular (b) PI/PVDF/PI, (c) OS/PVDF/OS, and (d) NL/PVDF/NL films foamed under different conditions: (subscript 1) 16 MPa, 163 °C, (subscript 2) 20 MPa, 163 °C, and (subscript 3) 20 MPa, 166 °C.
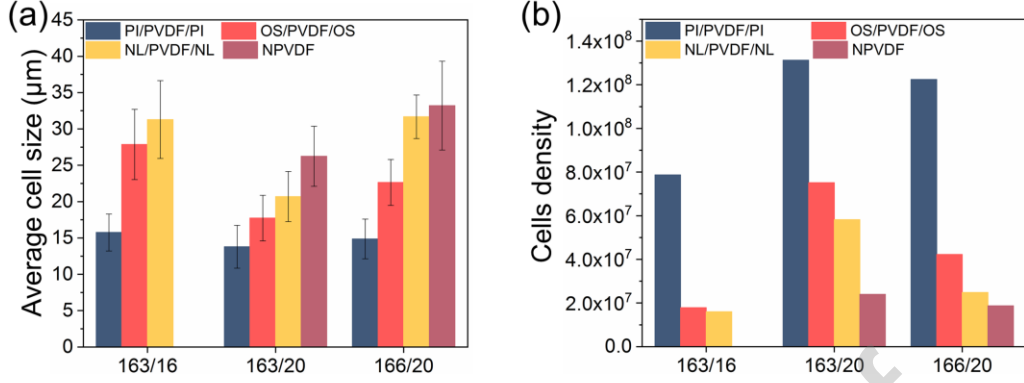
Figure 7. (a) Average cell size and (b) cell density statistical results of different cellular PVDF films prepared under different foaming conditions in the cross-section.

3.3. Mechanism of the surface-constrained foaming process

The surface-constrained foaming process has demonstrated prominent effects on cellular morphology both on the surface and in the cross-section. The underlying mechanism could be attributed to the interfacial cell nucleation on the interface of PVDF and the confined layer dominated by heterogeneous nucleation effect, as well as the homogeneous nucleation that occurred in the core region [45]. According to the classical nucleation theory, the cell nucleation in polymer foaming involves volume energy change (ΔG_v) and the surface energy change (ΔG_s) [46-48], from which one could derive the activation energy barrier of cell nucleation in a heterogeneous system as shown in Equation (4),

$$\Delta G^*_{het} = \Delta G^*_{hom} S = \frac{16\pi\gamma_{pc}^3 S(\theta)}{3(\Delta P)^2} \tag{4}$$

Where, ΔP represents the pressures of the gas in the bubble, and γ_{PC} is the surface tension of the polymer-cell interface, $S(\theta)$ depends on the contact angle (θ) between the polymer and the third phase.

Hence, the cell nucleation rates in homogeneous and heterogeneous systems can be expressed as follows:

$$N_{\text{hom}} = Cfe^{\left(\frac{-\Delta G_{\text{hom}}^*}{kT}\right)} \tag{5}$$

$$N_{het} = Cfe^{\left(\frac{-\Delta G_{het}^*}{kT}\right)} \tag{6}$$

Where, N_{hom} is homogeneous nucleation rate, N_{het} is heterogeneous nucleation rate, C is the concentration of gas molecules in the polymer, f is a frequency factor for nucleation.

During the CO_2 foaming process, the CO_2 concentration would gradually decrease as it approaches the PVDF film surface due to the rapid escaping of CO_2 molecules in the depressurization stage [32]. The surface-constrained foaming utilizes gas barrier layers to restrict the diffusion of CO_2 and, thereby, enhance the cell nucleation rate.

The CO_2 diffusivity results (Figure 8a) showed that the PVDF had a relatively high diffusion rate of 9.95×10^{-10} m^2/s, and the CO_2 diffusion rates of PI and organosilicone were in the same order of magnitude. However, the nature latex had the lowest diffusion rate of 4.73×10^{-13} m^2/s. It has been reported that the diffusivity is affected by temperature and pressure, and it increases with increasing temperature and pressure [49, 50]. The CO_2 diffusion coefficient depends strongly on the temperature but weakly on the pressure [51]. The positive effect of constrained layers with low diffusivity has been verified in previous studies [35, 52]. It is expected that NL/PVDF/NL film would have the slowest CO_2 diffusion and the largest C value, especially in the region close to the surface, which resulted in the largest cell density of the cellular NL/PVDF/NL film. Regarding PI/PVDF/PI film, although it had a similar CO_2 diffusion rate, the high stiffness of PI barrier film led to the dissociation of PI film from PVDF film. On the

contrary, both organosilicone and latex films are highly elastic and in situ synthesized on the surface of PVDF film, which resulted in tight adhesion. As shown in Figure 9, the interface between PVDF and PI films were distinct in the PI/PVDF/PI sample with some micro gaps presented, while OS/PVDF/ OS and NL/PVDF/NL samples displayed tight bonding between the PVDF and constrained layers, which ensured high efficiency in preventing the escape of CO_2 during foaming. In addition, the peeling test showed that the adhesion of nature latex to PVDF was stronger than that of organosilicone and PI (Figure 9d), which was agreed with the microscope observations. Furthermore, the elastic nature of organosilicone and nature latex made it possible for them to expand with the PVDF film, which is desired to obtain skinless cellular PVDF films with uniform cell morphology on the whole surface.
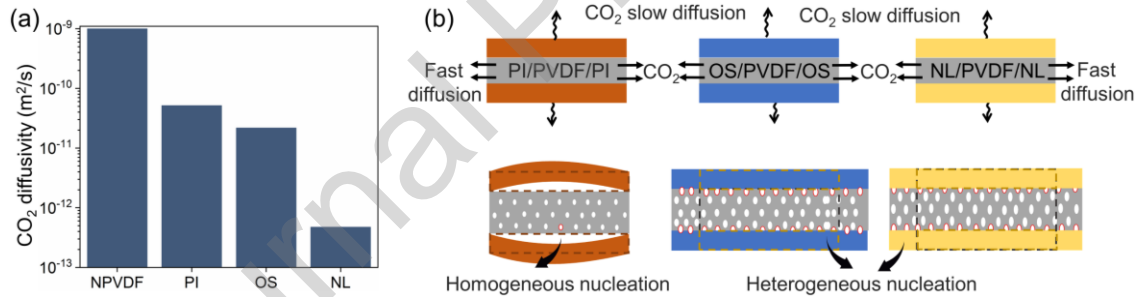
Figure 8. (a) CO_2 diffusivity of neat PVDF, PI, organosilicone, and nature latex films. (b) Schematic diagram of the mechanism for interfacial nucleation and diffusion-constrained cell growth in surface-constrained foaming using different gas barrier layers.
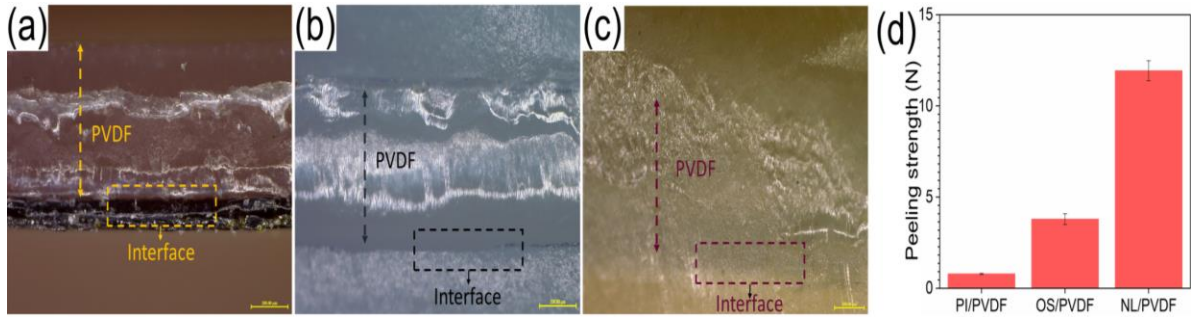
Figure 9. Optical images at the cross-section of (a) PI/PVDF/PI, (b) OS/PVDF/OS, and (c) NL/PVDF/NL showing the interfaces between the PVDF and constrained layers; (d) peeling strength of PI, OS, and NL adhered on PVDF before foaming.

The low CO_2 diffusion rate of latex resulted in a high cell nucleation rate, cell density, and small cell size on the surface of cellular NL/PVDF/NL film. However, the cell size and cell density in the cross-section of the cellular NL/PVDF/NL film showed the opposite trend among all surface-constrained films. This was because the heterogeneous nucleation on the interface had a much lower energy barrier than the homogenous nucleation in the core region, and the initially nucleated cells on the interface would trigger the diffusion of CO_2 towards the surface. The NL/PVDF/NL film had the strongest cell nucleation on the surface which resulted in the decrease of homogenous nucleation rate and the formation of fewer and larger cells in the core region. Therefore, the foaming behavior on the PVDF and barrier layer interface would affect the cellular structure in the core region, which resulted in different morphology changes of the skinless cellular PVDF films on the surface and the core region under different foaming conditions. When the foaming pressure was enhanced from 16 MPa to 20 MPa, the cell size in the core region was reduced by a significant increase of cell density due to the decrease of energy barrier (ΔG^{*}_{hom}) [44]. However, the cell size was greatly increased

on the surface of cellular OS/PVDF/OS and NL/PVDF/NL films. This was because the higher gas concentration at high pressure effectively increased the area that had been foamed on the PVDF surface. When the foaming temperature was increased from 163 °C to 166 °C, the cells in the core region became larger since the reduced surface tension of the polymer-cell interface would facilitate cell expansion and coalescence [44, 53].

In addition, the CO_2 diffusion at high temperature would be enhanced which may lead to an increase of C value at the interface of PVDF, and the barrier layer resulting in the further increase of cell nucleation rate. As demonstrated in the surface morphology evolvement of cellular OS/PVDF/OS and NL/PVDF/NL films, the foamed area on the film surface was greatly increased with an increase of foaming pressure and temperature (c.f. Figure 2-4). Moreover, conventional cellular PVDF film and cellular OS/PVDF/OS film not only displayed solid skin layers but also had a distinct cell size variation close to the surface as shown in Figures 10a and 10b, which was because of the CO_2 gas gradient in the region close to the surface caused by CO_2 escaping. Noticeably, both cellular OS/PVDF/OS (Figure 10c) and NL/PVDF/NL (Figure 10d) films had negligible cell size gradients across the region close to the surface, which could be attributed to the excellent gas barrier effect of organosilicone and nature latex layers.
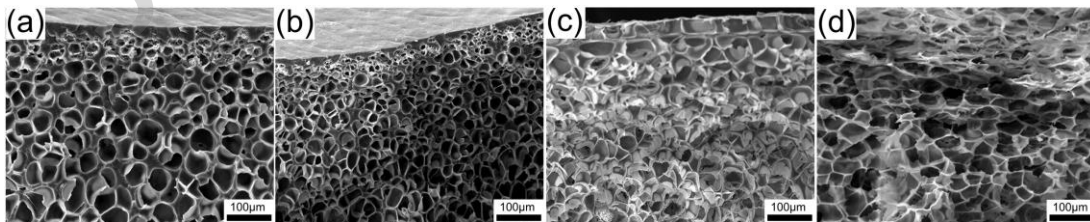

Figure 10. Cross-sectional SEM micrographs of (a) neat PVDF, cellular (b) PI/PVDF/PI, (c) OS/PVDF/OS, and (d) NL/PVDF/NL films foamed under 20 MPa at 166 °C showing the cell size gradient close to the surface.

3.4. Thermal properties of different cellular PVDF films

It is known that $scCO_2$ has a distinct plasticizing effect on polymer molecules and may affect their thermal properties [54, 55]. The sorption of CO_2 into polymers results in swelling and changes in the mechanical and physical properties of those polymers. The most important effect is the reduction of the glass transition temperature (T_g) of glassy polymers subjected to $scCO_2$, often simply called plasticization [56]. The plasticization of polymers is characterized by an increase in segmental and chain mobility. The plasticizing effect of CO_2 is the result of the ability of CO_2 molecules to interact with the sites in polymer molecules. It has also been shown experimentally that $scCO_2$ can interact with the C–F bond of PVDF, facilitating the dissolution of CO_2 as a blowing agent [42]. The melting and crystallization behaviors of different cellular PVDF films were analyzed using DSC. As shown in Figure 11a, all samples had two melting peaks that were assigned to the two major PVDF crystal phases, and both peaks were shifted to a higher temperature when processed with CO_2 foaming. Two endothermic peaks were observed after heating (labeled as T_{m1} and T_{m2} in the order of temperature from low to high). By analyzing T_{m1} and T_{m2} (Figure 11b), it was found that the cellular PVDF films with surface-constrained layers had much higher melting temperatures than conventional foamed films with the T_m of NL/PVDF/NL film been the highest. The crystallinity (χ_c) calculated from the heating curves (Figure 11c) showed that χ_c of the cellular films with surface-constrained layers was also higher than the unfoamed and conventional foamed PVDF. These results indicated that the $scCO_2$ molecules have interacted with the groups on the PVDF molecular chain and played a plasticizing role [57, 58], which increased the

21

free volume of the polymer and facilitated the crystallization of PVDF molecular chains. Moreover, the highest T_m and χ_c of NL/PVDF/NL film suggested that the slow diffusion of CO_2 during the foaming stage would give the PVDF molecules more time to rearrange into crystallites and is beneficial for enhancing the crystallinity. In the cooling curve (Figure 11d), all scCO$_2$ foamed samples had lower crystallization temperatures (T_c) than the unfoamed PVDF although the thermal history has been removed in the heating cycle, indicating enhanced molecular chain mobility. Since all polymers were heated up to 250 °C, any residual structure information will be lost and residual CO_2 escapes from the matrix. With the collapse of the cellular structure in the first heating, the plasticizing effect of CO_2 will no longer exist. Compared with unfoamed samples, foamed samples will form imperfect crystals during cooling due to the loss of CO_2 in the process of eliminating porous structure, resulting in lower T_c. At the same time, T_c will decrease with an increase of pressure caused by the residual CO_2 in the sealed crucible with the temperature increase [59-61]. However, the difference between the conventional foamed and surface-constrained foamed samples was eliminated. These results revealed that the surface-constrained foaming of PVDF could be an effective approach to elevate the crystallinity of cellular PVDF films.

22
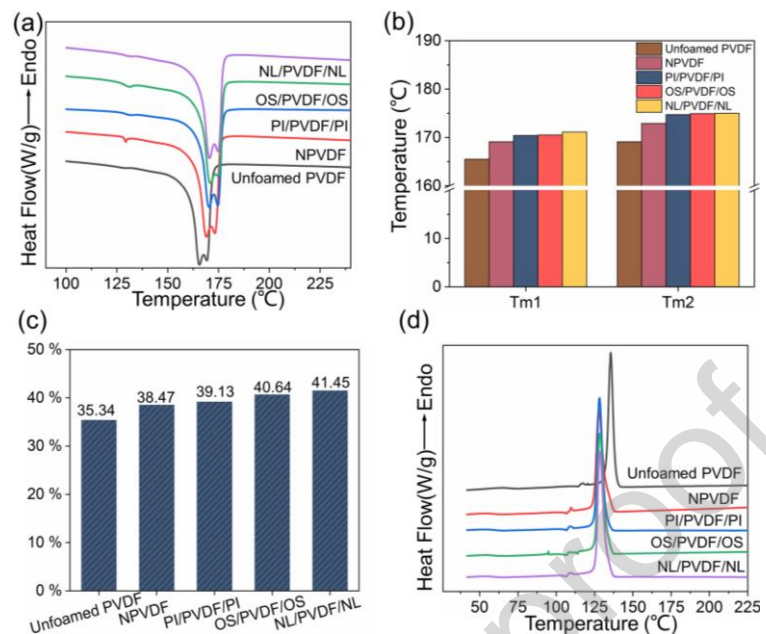
Figure 11. (a) DSC heating curves, (b) T_{m1} and T_{m2} values measured from the endothermic peaks of the DSC heating curves, (c) crystallinity measured from the heating curves, and (d) DSC cooling curves of unfoamed PVDF, conventional foamed PVDF film, and cellular PVDF films prepared by surface-constrained foaming.

Conclusions

Skinless cellular PVDF films were fabricated via surface-constrained scCO$_2$ foaming technique by using PI, organosilicone, and nature latex as gas barrier layers to prevent the fast escaping of CO$_2$ gas in the depressurization stage. Highly porous surfaces with uniform cell distribution across the whole film were produced attributing to the high interfacial adhesion and elasticity of organosilicone and nature latex. The interface between the PVDF and the barrier layers provided sites for heterogeneous cell nucleation and restricted the diffusion of CO$_2$, which resulted in the formation of numerous cells on the PVDF film surface. High cell nucleation rate on the interface would promote CO$_2$ diffusion to the surface region which led to the formation of relatively large cells in the

23

core region. The skin layer and cell size gradient in the region close to the surface were eliminated under the foaming conditions of 166 °C and 20 MPa using organosilicone and nature latex as the gas barrier layers. In addition, the lower CO_2 diffusion rate of nature latex contributed to higher CO_2 concentration and more cell nucleation sites on the interface, which resulted in smaller cell size on the surface compared with cellular PVDF film using organosilicone as the barrier layer. Moreover, the fabricated skinless cellular PVDF films exhibited superior thermal properties than the conventional PVDF foam due to the plasticizing effect of $scCO_2$ and the prolonged CO_2 diffusion time by the gas barrier layers. This study provides insights into the mechanism and influential factors of surface-constrained foaming and gives new thoughts for the fabrication of skinless polymer films by using $scCO_2$ foaming.

CRediT author statement

Lin Wang: Writing, data curation, visualization, investigation, formal analysis. **Wenhao Cui:** Investigation, formal analysis, visualization. **Hao-Yang Mi:** Writing-reviewing, funding acquisition, conceptualization, methodology. **Dongdong Hu:** Formal analysis, conceptualization. **Maxwell Fordjour Antwi-Afari:** Writing-reviewing, visualization. **Chuntai Liu:** Project administration, funding acquisition. **Changyu Shen:** Project administration, funding acquisition.

Declaration of Competing Interest

The authors declare that they have no known competing financial interests or personal relationships that could have appeared to influence the work reported in this paper.

Acknowledgment

Reference

[1] Y. Li, B. Shen, D. Yi, L. Zhang, W. Zhai, X. Wei, W. Zheng, The influence of gradient and sandwich configurations on the electromagnetic interference shielding performance of multilayered thermoplastic polyurethane/graphene composite foams, Compos. Sci. Technol., 138 (2017) 209-216.http://dx.doi.org/10.1016/j.compscitech.2016.12.002
[2] H.B. Zhang, Q. Yan, W.G. Zheng, Z. He, Z.Z. Yu, Tough graphene-polymer microcellular foams for electromagnetic interference shielding, ACS Appl. Mater. Interfaces, 3 (3)(2011) 918-924.http://dx.doi.org/10.1021/am200021v
[3] C. Wu, X. Huang, X. Wu, R. Qian, P. Jiang, Mechanically flexible and multifunctional polymer-based graphene foams for elastic conductors and oil-water separators, Adv. Mater., 25 (39)(2013) 5658-5662.http://dx.doi.org/10.1002/adma.201302406
[4] D.W. Kim, K. Eum, H. Kim, D. Kim, M.D.d. Mello, K. Park, M. Tsapatsis, Continuous ZIF-8/reduced graphene oxide nanocoating for ultrafast oil/water separation, Chem. Eng. J., 372 (2019) 509-515.http://dx.doi.org/10.1016/j.cej.2019.04.179
[5] B. Dong, Y. Guo, S. Sun, H.Y. Mi, P. He, M.F. Antwi-Afari, C. Liu, C. Shen, Shish-kebab-structured UHMWPE coating for efficient and cost-effective oil-water separation, ACS Appl. Mater. Interfaces, 12 (52)(2020) 58252-58262.http://dx.doi.org/10.1021/acsami.0c17900
[6] G. Ni, X. Zhu, H. Mi, P. Feng, J. Li, X. Jing, B. Dong, C. Liu, C. Shen, Skinless porous films generated by supercritical CO_2 foaming for high-performance complementary shaped triboelectric nanogenerators and self-powered sensors, Nano Energy, 87 (2021) 106148.http://dx.doi.org/10.1016/j.nanoen.2021.106148

[7] Y. Shao, C. Luo, B. Deng, B. Yin, M. Yang, Flexible porous silicone rubber-nanofiber nanocomposites generated by supercritical carbon dioxide foaming for harvesting mechanical energy, Nano Energy, 67 (2020) 104290.http://dx.doi.org/10.1016/j.nanoen.2019.104290

[8] X. Fan, G. Zhang, Q. Gao, J. Li, Z. Shang, H. Zhang, Y. Zhang, X. Shi, J. Qin, Highly expansive, thermally insulating epoxy/Ag nanosheet composite foam for electromagnetic interference shielding, Chem. Eng. J., 372 (2019) 191-202.http://dx.doi.org/10.1016/j.cej.2019.04.069

[9] P. Gong, S. Zhai, R. Lee, C. Zhao, P. Buahom, G. Li, C.B. Park, Environmentally friendly polylactic acid-based thermal insulation foams blown with supercritical CO_2, Ind. Eng. Chem. Res., 57 (15)(2018) 5464-5471.http://dx.doi.org/10.1021/acs.iecr.7b05023

[10] S. Zhang, Y. Zhao, X. Du, Y. Chu, S. Zhang, J. Huang, Gas sensors based on nano/microstructured organic field-effect transistors, Small, 15 (12)(2019) 1805196.http://dx.doi.org/10.1002/smll.201805196

[11] C. Lu, C. Shih, C. Chen, A. Chin, W. Su, Tuning the morphology of isoindigo donor-acceptor polymer film for high sensitivity ammonia sensor, Adv. Funct. Mater., 28 (40)(2018) 1803145.http://dx.doi.org/10.1002/adfm.201803145

[12] Q. Li, G. Chen, Y. Cui, S. Ji, Z. Liu, C. Wan, Y. Liu, Y. Lu, C. Wang, N. Zhang, Y. Cheng, K.Q. Zhang, X. Chen, Highly thermal-wet comfortable and conformal silk-based electrodes for on-skin sensors with sweat tolerance, ACS nano, 15 (6)(2021) 9955-9966.http://dx.doi.org/10.1021/acsnano.1c01431

[13] Z. Jiang, M.O.G. Nayeem, K. Fukuda, S. Ding, H. Jin, T. Yokota, D. Inoue, D. Hashizume, T. Someya, Highly stretchable metallic nanowire networks reinforced by the underlying randomly distributed elastic polymer nanofibers via interfacial adhesion improvement, Adv. Mater., 31 (37)(2019) 1903446.http://dx.doi.org/10.1002/adma.201903446

[14] Q. Dai, Z. Liu, L. Huang, C. Wang, Y. Zhao, Q. Fu, A. Zheng, H. Zhang, X. Li, Thin-film composite membrane breaking the trade-off between conductivity and selectivity for a flow battery, Nat. Commun., 11 (1)(2020) 13.http://dx.doi.org/10.1038/s41467-019-13704-2

[15] C. Li, X. Li, Q. Yang, P. Sun, L. Wu, B. Nie, H. Tian, Y. Wang, C. Wang, X. Chen, J. Shao, Tuning the mechanical and electrical properties of porous electrodes for architecting 3D microsupercapacitors with batteries-level energy, Adv. Sci., 8 (15)(2021) 2004957.http://dx.doi.org/10.1002/advs.202004957

[16] J. Mandal, Y. Fu, A.C. Overvig, M. Jia, K. Sun, N.N. Shi, H. Zhou, X. Xiao, N. Yu, Y. Yang, Hierarchically porous polymer coatings for highly efficient passive daytime radiative cooling, Science, 362 (6412)(2018) 315-319.http://dx.doi.org/10.1126/science.aat9513

[17] L. Zhao, L. Wang, Y. Zheng, S. Zhao, W. Wei, D. Zhang, X. Fu, K. Jiang, G. Shen, W. Han, Highly-stable polymer-crosslinked 2D MXene-based flexible biocompatible electronic skins for in vivo biomonitoring, Nano Energy, 84 (2021) 105921.http://dx.doi.org/10.1016/j.nanoen.2021.105921

[18] Y. Zhu, D. Joralmon, W. Shan, Y. Chen, J. Rong, H. Zhao, S. Xiao, X. Li, 3D printing biomimetic materials and structures for biomedical applications, Bio-Des. Manuf., 4 (2)(2021) 405-428.http://dx.doi.org/10.1007/s42242-020-00117-0

[19] X. Li, Y. Yuan, L. Liu, Y. Leung, Y. Chen, Y. Guo, Y. Chai, Y. Chen, 3D printing of hydroxyapatite/tricalcium phosphate scaffold with hierarchical porous structure for bone regeneration, Bio-Des. Manuf., 3 (1)(2019) 15-29.http://dx.doi.org/10.1007/s42242-019-00056-5

[20] M.G. Buonomenna, P. Macchi, M. Davoli, E. Drioli, Poly(vinylidene fluoride) membranes by phase inversion: the role the casting and coagulation conditions play in their morphology, crystalline structure and properties, Eur. Polym. J., 43 (4)(2007) 1557-1572.http://dx.doi.org/10.1016/j.eurpolymj.2006.12.033

[21] L. Li, T. Nemoto, K. Sugiyama, H. Yokoyama, CO_2 foaming in thin films of block copolymer containing fluorinated block, Macromolecules, 39 (14)(2006) 4746-4755.http://dx.doi.org/10.1021/ma060325l

[22] N. Thadavirul, P. Pavasant, P. Supaphol, Development of polycaprolactone porous scaffolds by combining solvent casting, particulate leaching, and polymer leaching techniques for bone tissue engineering, J. Biomed. Mater. Res. Part A, 102 (10)(2014) 3379-3392.http://dx.doi.org/10.1002/jbm.a.35010

[23] S.J. Lee, S.H. Oh, J. Liu, S. Soker, A. Atala, J.J. Yoo, The use of thermal treatments to enhance the mechanical properties of electrospun poly(epsilon-caprolactone) scaffolds, Biomaterials, 29 (10)(2008) 1422-1430.http://dx.doi.org/10.1016/j.biomaterials.2007.11.024

[24] X. Lei, C. Shao, X. Shou, K. Shi, L. Shi, Y. Zhao, Porous hydrogel arrays for hepatoma cell spheroid formation and drug resistance investigation, Bio-Des. Manuf., 4 (4)(2021) 842-850.http://dx.doi.org/10.1007/s42242-021-00141-8

[25] M.T. Gokmen, F.E. Du Prez, Porous polymer particles—a comprehensive guide to synthesis, characterization, functionalization and applications, Prog. Polym. Sci., 37 (3)(2012) 365-405.http://dx.doi.org/10.1016/j.progpolymsci.2011.07.006

[26] C. Thies, I.R. Dos Santos, J. Richard, V. VandeVelde, H. Rolland, J.-P. Benoit, A supercritical fluid-based coating technology 1: Process considerations, J. Microencapsul., 20 (1)(2003) 87-96.http://dx.doi.org/10.3109/02652040309178051

[27] V. Kumar, J.E. Weller, A model for the unfoamed skin on microcellular foams, Polym. Eng. Sci., 34 (3)(1994) 169-173.http://dx.doi.org/10.1002/pen.760340302

[28] H. Li, T.K. Sinha, J.S. Oh, J.K. Kim, Soft and flexible bilayer thermoplastic polyurethane foam for development of bioinspired artificial skin, ACS Appl. Mater. Interfaces, 10 (16)(2018) 14008-14016.http://dx.doi.org/10.1021/acsami.8b01026

[29] S. Siripurapu, J.A. Coughlan, R.J. Spontak, S.A. Khan, Surface-constrained foaming of polymer thin films with supercritical carbon dioxide, Macromolecules, 37 (26)(2004) 9872-9879.http://dx.doi.org/10.1021/ma0484983

[30] H. Mi, X. Jing, M.R. Salick, X. Peng, L. Turng, A novel thermoplastic polyurethane scaffold fabrication method based on injection foaming with water and supercritical carbon dioxide as coblowing agents, Polym. Eng. Sci., 54 (12)(2014) 2947-2957.http://dx.doi.org/10.1002/pen.23852

[31] J. Chen, J. Ye, X. Liao, S. Li, W. Xiao, Q. Yang, G. Li, Organic solvent free preparation of porous scaffolds based on the phase morphology control using supercritical CO_2, J. Supercrit. Fluids, 149 (2019) 88-96.http://dx.doi.org/10.1016/j.supflu.2019.03.021

[32] S. Siripurapu, J.M. DeSimone, S.A. Khan, R.J. Spontak, Low-temperature, surface-mediated foaming of polymer films, Adv. Mater., 16 (12)(2004) 989-994.http://dx.doi.org/10.1002/adma.200306068

[33] C. Ge, W. Zhai, Cellular thermoplastic polyurethane thin film: preparation, elasticity, and thermal insulation performance, Ind. Eng. Chem. Res., 57 (13)(2018) 4688-4696.http://dx.doi.org/10.1021/acs.iecr.7b05037

[34] C. Ge, W. Zhai, C.B. Park, Preparation of thermoplastic polyurethane (TPU) perforated membrane via CO_2 foaming and its particle separation performance, Polymers, 11 (5)(2019) 847.http://dx.doi.org/10.3390/polym11050847

[35] J. Li, X. Liao, Q. Jiang, W. Wang, G. Li, Creating orientated cellular structure in thermoplastic polyurethane through strong interfacial shear interaction and supercritical carbon dioxide foaming for largely improving the foam compression performance, J. Supercrit. Fluids, 153 (2019) 104577.http://dx.doi.org/10.1016/j.supflu.2019.104577

[36] T. Yuan, J. Meng, T. Hao, Z. Wang, Y. Zhang, A scalable method toward superhydrophilic and underwater superoleophobic PVDF membranes for effective oil/water emulsion separation, ACS Appl. Mater. Interfaces, 7 (27)(2015) 14896-14904.http://dx.doi.org/10.1021/acsami.5b03625

[37] L. Wang, W.F. Yong, L.E. Yu, T. Chung, Design of high efficiency PVDF-PEG hollow fibers for air filtration of ultrafine particles, J. Membr. Sci., 535 (2017) 342-349.http://dx.doi.org/10.1016/j.memsci.2017.04.053

[38] B. Zhao, C. Zhao, C. Wang, C.B. Park, Poly(vinylidene fluoride) foams: a promising low-k dielectric and heat-insulating material, J. Mater. Chem. C, 6 (12)(2018) 3065-3073.http://dx.doi.org/10.1039/c8tc00547h

[39] V. Jella, S. Ippili, J. Eom, J. Choi, S. Yoon, Enhanced output performance of a flexible piezoelectric energy harvester based on stable MAPbI3-PVDF composite films, Nano Energy, 53 (2018) 46-56.http://dx.doi.org/10.1016/j.nanoen.2018.08.033

[40] J.E. Lee, Y. Guo, R.E. Lee, S.N. Leung, Fabrication of electroactive poly(vinylidene fluoride) through non-isothermal crystallization and supercritical CO_2 processing, RSC Adv., 7 (77)(2017) 48712-48722.http://dx.doi.org/10.1039/c7ra09162a

[41] J.C.H. Wong, E. Tervoort, S. Busato, U.T. Gonzenbach, A.R. Studart, P. Ermanni, L.J. Gauckler, Macroporous polymers from particle-stabilized foams, J. Mater. Chem., 19 (29)(2009) 5129.http://dx.doi.org/10.1039/b908926h

[42] C. Yang, N. Chen, X. Liu, Q. Wang, C. Zhang, Coupling selective laser sintering and supercritical CO_2 foaming for 3D printed porous polyvinylidene fluoride with improved piezoelectric performance, RSC Adv., 11 (34)(2021) 20662-20669.http://dx.doi.org/10.1039/d1ra03341g

[43] K. Nakagawa, Y. Ishida, Annealing effects in poly (vinylidene fluoride) as revealed by specific volume measurements, differential scanning calorimetry, and electron microscopy, J. Polym. Sci., 11 (11)(1973) 2153-2171.http://dx.doi.org/10.1002/pol.1973.180111107

[44] S.N. Leung, A. Wong, Q. Guo, C.B. Park, J.H. Zong, Change in the critical nucleation radius and its impact on cell stability during polymeric foaming processes, Chem. Eng. Sci., 64 (23)(2009) 4899-4907.http://dx.doi.org/10.1016/j.ces.2009.07.025

[45] W. Zhai, H. Wang, J. Yu, J. Dong, J. He, Foaming behavior of polypropylene/polystyrene blends enhanced by improved interfacial compatibility, Polym. Sci. Pt. B-Polym. Phys., 46 (16)(2008) 1641-1651.http://dx.doi.org/10.1002/polb.21498

[46] J. Colton, N. Suh, The nucleation of microcellular thermoplastic foam with additives: part I: theoretical considerations, Polym. Eng. Sci., 27 (7)(1987) 485-492.http://dx.doi.org/10.1002/pen.760270702

[47] J. Colton, N. Suh, The nucleation of microcellular thermoplastic foam with additives: part II: experimental results and discussion, Polym. Eng. Sci., 27 (7)(1987) 493-499.http://dx.doi.org/10.1002/pen.760270703

[48] J.S. Colton, N.P. Suh, Nucleation of microcellular foam: theory and practice, Polym. Eng. Sci., 27 (7)(1987) 500-503.http://dx.doi.org/10.1002/pen.760270704

[49] R. Li, J.H. Lee, C. Wang, L. Howe Mark, C.B. Park, Solubility and diffusivity of CO_2 and N_2 in TPU and their effects on cell nucleation in batch foaming, J. Supercrit. Fluids, 154 (2019) 104623.http://dx.doi.org/10.1016/j.supflu.2019.104623

[50] M.N. Amar, A. Jahanbani Ghahfarokhi, Prediction of CO_2 diffusivity in brine using white-box machine learning, J. Pet. Sci. Eng., 190 (2020) 107037.http://dx.doi.org/10.1016/j.petrol.2020.107037

[51] R. Li, N. Ye, V. Shaayegan, T. Fang, Experimental measurement of CO_2 diffusion in PMMA and its effect on microcellular foaming, J. Supercrit. Fluids, 135 (2018) 180-187.http://dx.doi.org/10.1016/j.supflu.2018.01.024

[52] J. Jiang, H. Zheng, H. Liu, W. Zhai, Tunable cell structure and mechanism in porous thermoplastic polyurethane micro-film fabricated by a diffusion-restricted physical foaming process, J. Supercrit. Fluids, 171 (2021) 105205.http://dx.doi.org/10.1016/j.supflu.2021.105205

[53] H. Park, R. Thompson, N. Lanson, C. Tzoganakis, C. Park, P. Chen, Effect of temperature and pressure on surface tension of polystyrene in supercritical carbon dioxide, J. Phys. Chem. B, 111 (15)(2007) 3859-3868.http://dx.doi.org/10.1021/jp065851t

[54] M. Nofar, W. Zhu, C.B. Park, Effect of dissolved CO_2 on the crystallization behavior of linear and branched PLA, Polymer, 53 (15)(2012) 3341-3353.http://dx.doi.org/10.1016/j.polymer.2012.04.054

[55] A.C. Paolo Alessi, Ireneo Kikic,Febe Vecchione, Plasticization of polymers with supercritical carbon dioxide: experimental determination of glass‐transition temperatures, J. Appl. Polym. Sci., 88 (9)(2003) 2189-2193.http://dx.doi.org/10.1002/app.11881

[56] K.S.G. Fleming O S, Polymer processing with supercritical fluids, Supercritical Carbon Dioxide, (2005) 205-238.http://dx.doi.org/10.1002/3527606726.ch10

[57] J.E. Lee, S.N. Leung, Multi-stage crystallization mechanism of electroactive phase polyvinylidene fluoride induced by thermal and supercritical carbon dioxide processing, Crystengcomm, 20 (29)(2018) 4080-4089.http://dx.doi.org/10.1039/c8ce00531a

[58] D. Xu, H. Zhang, L. Pu, L. Li, Fabrication of poly(vinylidene fluoride)/multiwalled carbon nanotube nanocomposite foam via supercritical fluid carbon dioxide: synergistic enhancement of piezoelectric and mechanical properties, Compos. Sci. Technol., 192 (2020) 108108.http://dx.doi.org/10.1016/j.compscitech.2020.108108

[59] D. Li, T. Liu, L. Zhao, X. Lian, W. Yuan, Foaming of Poly(lactic acid) based on its nonisothermal crystallization behavior under compressed carbon dioxide, Ind. Eng. Chem. Res., 50 (4)(2011) 1997-2007.http://dx.doi.org/10.1021/ie101723g

[60] L. Yu, H. Liu, K. Dean, Thermal behaviour of poly(lactic acid) in contact with compressed carbon dioxide, Polym. Int., 58 (4)(2009) 368-372.http://dx.doi.org/10.1002/pi.2540

[61] A. Ameli, M. Nofar, D. Jahani, G. Rizvi, C.B. Park, Development of high void fraction polylactide composite foams using injection molding: Crystallization and foaming behaviors, Chem. Eng. J., 262 (2015) 78-87.http://dx.doi.org/10.1016/j.cej.2014.09.087

Graphical abstract
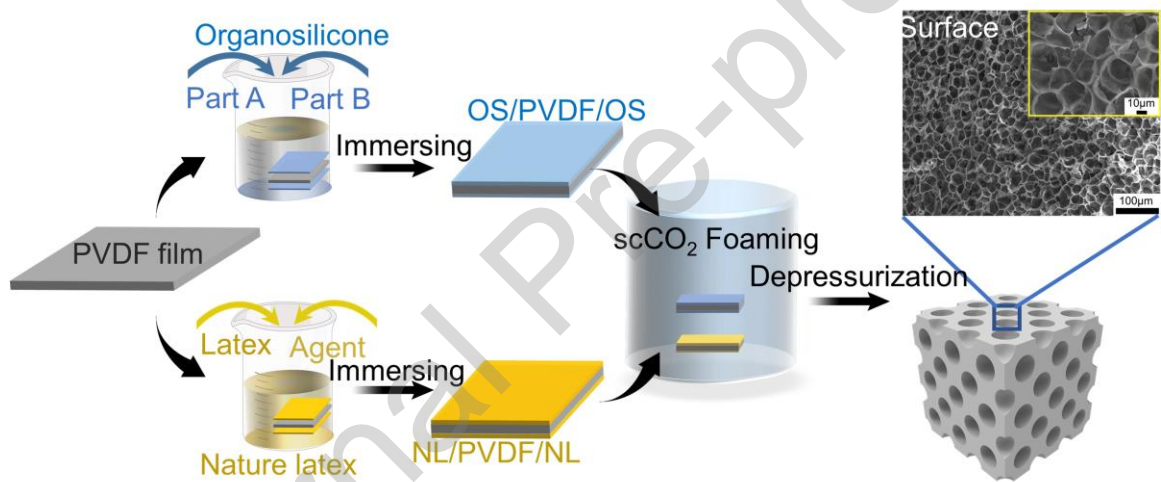
Declaration of interests

☒ The authors declare that they have no known competing financial interests or personal

relationships that could have appeared to influence the work reported in this paper.

☐The authors declare the following financial interests/personal relationships which may be
considered as potential competing interests:

Highlights

- Fabricating skinless PVDF cellular films via surface-constrained scCO$_2$ foaming

- Organosilicone and nature latex were used as constrained layers

- Low CO$_2$ diffusivity and high interfacial adhesion assisted cell nucleation

- Skinless PVDF cellular films have negligible cell size gradient close to surface

- Skinless PVDF cellular films exhibit enhanced cystallinity and melting temperature